An orthorhombic representation of a heterogeneous medium for the finite-difference modelling of seismic wave propagation

Jozef Kristek [1,2], Peter Moczo [1,2], Emmanuel Chaljub [3,4], Miriam Kristekova [2,1]

[1] *Faculty of Mathematics, Physics and Informatics, Comenius University Bratislava, Mlynska dolina F1, 842 48 Bratislava, Slovak Republic. E-mail: kristek@fmph.uniba.sk*

[2] *Earth Science Institute, Slovak Academy of Sciences, Dubravska cesta 9, 845 28 Bratislava, Slovak Republic*

[3] *Univ. Grenoble Alpes, ISTerre, F-38041 Grenoble, France*

[4] *CNRS, ISTerre, F-38041 Grenoble, France*

SUMMARY

The possibility of applying one explicit finite-difference scheme to all interior grid points (points not lying on a grid border) no matter what their positions are with respect to the material interface is one of the key factors of the computational efficiency of the finite-difference modelling. Smooth or discontinuous heterogeneity of the medium is accounted for only by values of the effective grid moduli and densities. Accuracy of modelling thus very much depends on how these effective grid parameters are evaluated. We present an orthorhombic representation of a heterogeneous medium for the finite-difference modelling. We numerically demonstrate its superior accuracy. Compared to the harmonic-averaging representation (Moczo et al. 2002) the orthorhombic representation is more accurate mainly in the case of strong surface waves that are especially important in local surface sedimentary basins.

The orthorhombic representation is applicable to modelling seismic wave propagation and earthquake motion in isotropic models with material interfaces and smooth heterogeneities using velocity-stress, displacement-stress and displacement FD schemes on staggered, partly-staggered, Lebedev and collocated grids.

Key words
Computational seismology; Theoretical seismology; Wave propagation; Numerical approximations and analysis; Earthquake ground motions

1 INTRODUCTION

Sufficiently realistic models are necessary for numerical modelling of seismic wave propagation as well as for prediction of earthquake ground motion especially in local surface sedimentary structures capable to produce anomalous earthquake motion. The realistic physical model has to be sufficiently accurately and efficiently represented by discrete grid models in the (spatial) domain numerical methods such as the finite-difference methods.

Models of the Earth's interior and surface geological structures have to include layers/blocks of different materials. Inside a layer/block, material parameters (P and S wave speeds, density, P and S wave quality factors) may change continuously. The material parameters may change discontinuously at a contact of two layers/blocks. In local surface sedimentary structures the ratio of the S wave speeds in the bedrock and sediments commonly reaches values considerably larger than 2, and even 10 is not exceptional. Large velocity contrasts at material interfaces can dominantly contribute to forming seismic wave propagation. It is therefore obvious that accuracy of representation of the interfaces in the discrete grid model considerably affects the overall accuracy of the numerical modelling.

Recent FD schemes represent a large variety of approaches with considerable differences in accuracy and computational efficiency in realistic models with large velocity contrasts and complex geometry of material interfaces. This is mainly due to a level of (in)consistency of the various discrete representations of the interfaces with the boundary conditions at the interfaces. Let us note that the FD schemes also differ in accuracy in models with large P-wave to S-wave speed ratio; see Moczo et al. (2010, 2011).

At the welded material interface the displacement or particle-velocity and traction vectors are continuous. Consequently, a discrete representation of a welded material interface in a grid should sufficiently well approximate the boundary conditions.

One possible approach is to apply different FD schemes to different grid points: a FD scheme for the smoothly heterogeneous medium to the grid points away of the interface, and specific FD schemes to the grid points at and near (this depends on the stencil) the interface. The latter schemes have to be obtained by a proper incorporation of the boundary conditions at the interface. Such approach has been called homogeneous. Clearly, the schemes are specific for a particular geometry of the interface. Whereas feasible for simple interface geometry, the application of the homogeneous approach to non-planar interfaces is difficult and therefore has been considered impractical. In any case, the approach requires stable and sufficiently accurate FD approximation of the boundary conditions which is not a trivial problem.

In the alternative heterogeneous approach only one FD scheme is used for all interior grid points (points not lying on boundaries of a grid) no matter what their positions are with respect to

the material interface. The presence of the interface is accounted for only by values of effective material parameters assigned to grid positions. Therefore, the heterogeneous approach has been commonly applied to incorporate both continuous and discontinuous heterogeneities of medium.

If a FD scheme should be applicable to any interior grid point, it should approximate equation of motion and stress-strain relation (SSR) valid for both the smoothly heterogeneous medium and interface. In other words, for finding a FD scheme applicable to the grid points at, near and away of the material interface we need SSR for a point at the interface that would a) have the same form as SSR for a point in a smooth medium and b) be consistent with the interface boundary conditions.

SSR (Hooke's law) for a smooth isotropic elastic medium may be written in the matrix form

$$\vec{\sigma} = \mathbf{E}\,\vec{\varepsilon} \tag{1.1}$$

where the stress vector, strain vector and elasticity matrix are, respectively,

$$\vec{\sigma} \equiv \left[\sigma_{xx}, \sigma_{yy}, \sigma_{zz}, \sigma_{xy}, \sigma_{yz}, \sigma_{zx}\right]^T, \quad \vec{\varepsilon} \equiv \left[\varepsilon_{xx}, \varepsilon_{yy}, \varepsilon_{zz}, \varepsilon_{xy}, \varepsilon_{yz}, \varepsilon_{zx}\right]^T \tag{1.2}$$

$$\mathbf{E} \equiv \begin{bmatrix} \lambda+2\mu & \lambda & \lambda & 0 & 0 & 0 \\ \lambda & \lambda+2\mu & \lambda & 0 & 0 & 0 \\ \lambda & \lambda & \lambda+2\mu & 0 & 0 & 0 \\ 0 & 0 & 0 & 2\mu & 0 & 0 \\ 0 & 0 & 0 & 0 & 2\mu & 0 \\ 0 & 0 & 0 & 0 & 0 & 2\mu \end{bmatrix} \tag{1.3}$$

(The defined quantities do not correspond to Voigt notation. This aspect is not important in the article.) Thus we need SSR for a point at an interface which has the same form as Hooke's law (1.1) for the considered stress and strain vectors. Although Backus (1962) and Schoenberg & Muir (1989) addressed the problem of the equivalent medium consistent with the interface boundary condition, and Muir et al. (1992) explicitly pointed out its relation to the FD schemes, apparently this fundamental task had not attracted sufficient attention of developers of FD schemes for several decades until the article by Moczo et al. (2002). They suggested a simplified approach for the (2,4) staggered-grid schemes: an effective grid elastic modulus at the grid position of the stress-tensor component evaluated as a volume integral harmonic average of the modulus within a volume of the grid cell centred at the grid position. Numerical tests confirmed that the scheme was more accurate than the staggered-grid schemes presented earlier. The historical overview can be found in the book by Moczo et al. (2014).

The SCEC (Southern California Earthquake Center) code comparative exercise (Day et al. 2003 and also Bielak et al. 2010) as well as the ESG2006 (ESG – Effects of Surface Geology 2006) international comparative exercise for a typical deep Alpine Grenoble valley, France

(Chaljub et al. 2006, Tsuno et al. 2006, Chaljub et al. 2010) clearly demonstrated that it had been far from trivial to reach satisfactory level of agreement among numerical predictions by different methods and, specifically among predictions by different FD schemes. In the ESG2006 only four predictions reached a reasonable level of agreement, the FD predictions based on approach by Moczo et al. (2002) among them. See the article by Chaljub et al. (2010) for details.

The direct impulse for developing a new discrete representation of material interface came from the quantitative iterative analysis of numerical predictions in the unprecedented international comparative E2VP exercise (E2VP – Euroseistest Verification and Validation Project 2008-2012; Chaljub et al. 2015, Maufroy et al. 2015) for the shallow sedimentary Mygdonian basin, Greece. The iterative analysis eventually included a set of complex realistic models and a set of related canonical models. The stringent canonical models made it possible to identify insufficient accuracy in the FD modelling of strong surface waves along horizontal interface with large velocity contrast. This is understandable – the harmonic averaging is strictly accurate only in 1D problem. In the previous reported modelling studies the approximate discrete representation by Moczo et al. (2002) based on volume harmonic averaging proved sufficiently accurate. The reason was that the simulated wavefields were not so strongly dominated by surface waves propagating along horizontal material interfaces.

Let us eventually mention the general alternative homogenization approach for effective representation of medium heterogeneity developed by Capdeville and his colleagues (e.g., Capdeville and Marigo 2007; Capdeville et al. 2013).

For treating material heterogeneity in the spectral-element, discontinuous Galerkin, and pseudospectral methods we refer to the articles by Chaljub et al. (2010, 2015) and relevant chapters in the book by Moczo et al. (2014). These references are also relevant for the FD method.

First we explain SSR for a point at the planar material interface parallel to a Cartesian coordinate plane. We present an alternative (as compared to Moczo et al. 2002) derivation that makes it possible to identify the resulting effective discrete representation in relation to continuous and discontinuous field quantities. The derivation provides the necessary basis for the new representation. Then we consider shear and normal stress-tensor components in a heterogeneous cell. We present and discuss effective representation of a heterogeneous grid cell based on orthorhombic averaging. We demonstrate the accuracy of the representation by numerical tests.

2 THE STRESS-STRAIN RELATION (SSR) FOR A PLANAR MATERIAL INTERFACE

Consider a planar welded interface parallel to a Cartesian coordinate plane. Continuity of displacement implies continuity of three strain-tensor components, and continuity of traction implies continuity of three stress-tensor components across the interface. Fig. 1 summarizes continuous and discontinuous stress- and strain-tensor components for the three Cartesian orientations. In the following sections we analyse the shear and normal stresses in terms of discontinuous and continuous components.

interface perpendicular to the					
x axis		y axis		z axis	
continuous	discontinuous	continuous	discontinuous	continuous	discontinuous
σ_{xx}	ε_{xx}	σ_{yy}	ε_{yy}	σ_{zz}	ε_{zz}
σ_{xy}	ε_{xy}	σ_{yz}	ε_{yz}	σ_{zx}	ε_{zx}
σ_{zx}	ε_{zx}	σ_{xy}	ε_{xy}	σ_{yz}	ε_{yz}
ε_{yy}	σ_{yy}	ε_{zz}	σ_{zz}	ε_{xx}	σ_{xx}
ε_{zz}	σ_{zz}	ε_{xx}	σ_{xx}	ε_{yy}	σ_{yy}
ε_{yz}	σ_{yz}	ε_{zx}	σ_{zx}	ε_{xy}	σ_{xy}

Figure 1. Continuous and discontinuous stress- and strain-tensor components for the three Cartesian orientations of a material interface.

2.1. Shear stress-tensor components at an interface perpendicular to the x axis

Discontinuous shear stress-tensor component. For the two halfspaces (indicated by the $-$ and $+$ superscripts) in a welded contact we can write in general

$$\begin{aligned} \sigma_{yz}^{-} &= 2\mu^{-}\,\varepsilon_{yz} \\ \sigma_{yz}^{+} &= 2\mu^{+}\,\varepsilon_{yz} \end{aligned} \tag{2.1}$$

Considering continuity of ε_{yz} and an arithmetic average $\left\langle \sigma_{yz} \right\rangle^{x}$ of the stress-tensor components at the interface,

$$\left\langle \sigma_{yz} \right\rangle^{x} \equiv \tfrac{1}{2}\left(\sigma_{yz}^{-} + \sigma_{yz}^{+} \right) , \tag{2.2}$$

the summation of Eqs. (2.1) leads to SSR

$$\left\langle \sigma_{yz} \right\rangle^{x} = 2 \left\langle \mu \right\rangle^{x} \varepsilon_{yz} , \tag{2.3}$$

with the arithmetic average of the shear moduli

$$\left\langle \mu \right\rangle^{x} \equiv \tfrac{1}{2}\left(\mu^{-} + \mu^{+} \right). \tag{2.4}$$

Continuous stress-tensor components. For example, for σ_{xy} we may write

$$\begin{aligned} \sigma_{xy} &= 2\mu^{-} \varepsilon_{xy}^{-} \\ \sigma_{xy} &= 2\mu^{+} \varepsilon_{xy}^{+} \end{aligned} \tag{2.5}$$

or

$$\begin{aligned} \frac{1}{\mu^{-}} \sigma_{xy} &= 2 \varepsilon_{xy}^{-} \\ \frac{1}{\mu^{+}} \sigma_{xy} &= 2 \varepsilon_{xy}^{+} \end{aligned} \tag{2.6}$$

Considering continuity of σ_{xy} and an arithmetic average $\left\langle \varepsilon_{xy} \right\rangle^{x}$ at the interface,

$$\left\langle \varepsilon_{xy} \right\rangle^{x} \equiv \tfrac{1}{2}\left(\varepsilon_{xy}^{-} + \varepsilon_{xy}^{+} \right) \tag{2.7}$$

the summation of Eqs. (2.6) leads to SSR

$$\sigma_{xy} = 2 \left\langle \mu \right\rangle^{Hx} \left\langle \varepsilon_{xy} \right\rangle^{x} \tag{2.8}$$

with the harmonic average of the shear moduli

$$\left\langle \mu \right\rangle^{Hx} \equiv \frac{2}{\dfrac{1}{\mu^{-}} + \dfrac{1}{\mu^{+}}} \tag{2.9}$$

Analogously we obtain a relation for σ_{zx}. The relations for the shear stress-tensor components at the interface perpendicular to the x axis are then

$$\begin{aligned} \sigma_{xy} &= 2 \left\langle \mu \right\rangle^{Hx} \left\langle \varepsilon_{xy} \right\rangle^{x} \\ \left\langle \sigma_{yz} \right\rangle^{x} &= 2 \left\langle \mu \right\rangle^{x} \quad \varepsilon_{yz} \\ \sigma_{zx} &= 2 \left\langle \mu \right\rangle^{Hx} \left\langle \varepsilon_{zx} \right\rangle^{x} \end{aligned} \tag{2.10}$$

Partial summary. SSRs for the shear stress-tensor components at the interface perpendicular to the x-axis:

- Continuity of ε_{yz} and the arithmetic averaging of the discontinuous σ_{yz} imply the arithmetic averaging of the shear moduli, $\langle \mu \rangle^{x}$.
- Continuity of σ_{xy} (or σ_{zx}) and the arithmetic averaging of the discontinuous ε_{xy} (or ε_{zx}) imply the harmonic averaging of the shear moduli, $\langle \mu \rangle^{Hx}$.
- SSRs (2.10) have the same forms as SSRs for a point in a smooth medium and are consistent with the interface boundary conditions.

2.2. Normal stress-tensor components at an interface perpendicular to the x axis

SSRs in a smooth medium are:

$$\begin{aligned} \sigma_{xx} &= M\,\varepsilon_{xx} + \lambda\,\varepsilon_{yy} + \lambda\,\varepsilon_{zz} \\ \sigma_{yy} &= \lambda\,\varepsilon_{xx} + M\,\varepsilon_{yy} + \lambda\,\varepsilon_{zz} \\ \sigma_{zz} &= \lambda\,\varepsilon_{xx} + \lambda\,\varepsilon_{yy} + M\,\varepsilon_{zz} \end{aligned} \tag{2.11}$$

Here

$$M \equiv \lambda + 2\mu \tag{2.12}$$

For two halfspaces in contact we may write

$$\begin{aligned} \sigma_{xx} &= M^{-}\,\varepsilon_{xx}^{-} + \lambda^{-}\varepsilon_{yy} + \lambda^{-}\varepsilon_{zz} \\ \sigma_{xx} &= M^{+}\,\varepsilon_{xx}^{+} + \lambda^{+}\varepsilon_{yy} + \lambda^{+}\varepsilon_{zz} \end{aligned} \tag{2.13}$$

$$\begin{aligned} \sigma_{yy}^{-} &= \lambda^{-}\varepsilon_{xx}^{-} + M^{-}\varepsilon_{yy} + \lambda^{-}\varepsilon_{zz} \\ \sigma_{yy}^{+} &= \lambda^{+}\varepsilon_{xx}^{+} + M^{+}\varepsilon_{yy} + \lambda^{+}\varepsilon_{zz} \end{aligned} \tag{2.14}$$

$$\begin{aligned} \sigma_{zz}^{-} &= \lambda^{-}\varepsilon_{xx}^{-} + \lambda^{-}\varepsilon_{yy} + M^{-}\,\varepsilon_{zz} \\ \sigma_{zz}^{+} &= \lambda^{+}\varepsilon_{xx}^{+} + \lambda^{+}\varepsilon_{yy} + M^{+}\,\varepsilon_{zz} \end{aligned} \tag{2.15}$$

Continuous stress-tensor component. Because the interface is perpendicular to the x axis, relations for σ_{xx} are simpler for averaging compared to σ_{yy} and σ_{zz}: they include only one discontinuous quantity – ε_{xx}. Relations (2.13) may be written as

$$\begin{aligned} \varepsilon_{xx}^{-} &= \frac{1}{M^{-}}\sigma_{xx} - \frac{\lambda^{-}}{M^{-}}\varepsilon_{yy} - \frac{\lambda^{-}}{M^{-}}\varepsilon_{zz} \\ \varepsilon_{xx}^{+} &= \frac{1}{M^{+}}\sigma_{xx} - \frac{\lambda^{+}}{M^{+}}\varepsilon_{yy} - \frac{\lambda^{+}}{M^{+}}\varepsilon_{zz} \end{aligned} \tag{2.16}$$

Continuity of σ_{xx}, ε_{yy} and ε_{zz}, and the arithmetic averaging of ε_{xx}^{-} and ε_{xx}^{+} lead to

$$\langle \varepsilon_{xx} \rangle^{x} = \left[\langle M \rangle^{Hx} \right]^{-1} \sigma_{xx} - \left\langle \frac{\lambda}{M} \right\rangle^{x} \varepsilon_{yy} - \left\langle \frac{\lambda}{M} \right\rangle^{x} \varepsilon_{zz} \tag{2.17}$$

and

$$\sigma_{xx} = \langle M \rangle^{Hx} \langle \varepsilon_{xx} \rangle^{x} + \left\langle \frac{\lambda}{M} \right\rangle^{x} \langle M \rangle^{Hx} \varepsilon_{yy} + \left\langle \frac{\lambda}{M} \right\rangle^{x} \langle M \rangle^{Hx} \varepsilon_{zz} \tag{2.18}$$

Discontinuous stress-tensor component. Consider, e.g., σ_{yy}. It is clear from Eqs. (2.14) that before we average σ_{yy}^{-} and σ_{yy}^{+}, we have to express ε_{xx}^{-} and ε_{xx}^{+} using continuous field quantities. Using (2.16) in (2.14) we obtain

$$\begin{aligned} \sigma_{yy}^{-} &= \frac{\lambda^{-}}{M^{-}} \sigma_{xx} + \left(M^{-} - \lambda^{-} \frac{\lambda^{-}}{M^{-}} \right) \varepsilon_{yy} + \left(\lambda^{-} - \lambda^{-} \frac{\lambda^{-}}{M^{-}} \right) \varepsilon_{zz} \\ \sigma_{yy}^{+} &= \frac{\lambda^{+}}{M^{+}} \sigma_{xx} + \left(M^{+} - \lambda^{+} \frac{\lambda^{+}}{M^{+}} \right) \varepsilon_{yy} + \left(\lambda^{+} - \lambda^{+} \frac{\lambda^{+}}{M^{+}} \right) \varepsilon_{zz} \end{aligned} \tag{2.19}$$

Continuity of σ_{xx}, ε_{yy} and ε_{zz}, and the arithmetic averaging of σ_{yy}^{-} and σ_{yy}^{+} give

$$\langle \sigma_{yy} \rangle^{x} = \left\langle \frac{\lambda}{M} \right\rangle^{x} \sigma_{xx} + \left[\langle M \rangle^{x} - \left\langle \frac{\lambda^{2}}{M} \right\rangle^{x} \right] \varepsilon_{yy} + \left[\langle \lambda \rangle^{x} - \left\langle \frac{\lambda^{2}}{M} \right\rangle^{x} \right] \varepsilon_{zz} \tag{2.20}$$

Substituting the r.h.s. of Eq. (2.18) for σ_{xx} gives the sought SSR

$$\begin{aligned} \langle \sigma_{yy} \rangle^{x} = & \left\langle \frac{\lambda}{M} \right\rangle^{x} \langle M \rangle^{Hx} \langle \varepsilon_{xx} \rangle \\ & + \left\{ \langle M \rangle^{x} - \left\langle \frac{\lambda^{2}}{M} \right\rangle^{x} + \left[\left\langle \frac{\lambda}{M} \right\rangle^{x} \right]^{2} \langle M \rangle^{Hx} \right\} \varepsilon_{yy} \\ & + \left\{ \langle \lambda \rangle^{x} - \left\langle \frac{\lambda^{2}}{M} \right\rangle^{x} + \left[\left\langle \frac{\lambda}{M} \right\rangle^{x} \right]^{2} \langle M \rangle^{Hx} \right\} \varepsilon_{zz} \end{aligned} \tag{2.21}$$

Analogously we easily obtain

$$\langle \sigma_{zz} \rangle^x = \left\langle \frac{\lambda}{M} \right\rangle^x \langle M \rangle^{Hx} \langle \varepsilon_{xx} \rangle + \left\{ \langle \lambda \rangle^x - \left\langle \frac{\lambda^2}{M} \right\rangle^x + \left[\left\langle \frac{\lambda}{M} \right\rangle^x \right]^2 \langle M \rangle^{Hx} \right\} \varepsilon_{yy} + \left\{ \langle M \rangle^x - \left\langle \frac{\lambda^2}{M} \right\rangle^x + \left[\left\langle \frac{\lambda}{M} \right\rangle^x \right]^2 \langle M \rangle^{Hx} \right\} \varepsilon_{zz} \tag{2.22}$$

Partial summary. SSRs for the normal stress-tensor components at the interface perpendicular to the x-axis:

- Continuity of σ_{xx}, ε_{yy} and ε_{zz}, and the arithmetic averaging of the discontinuous ε_{xx} imply two averaged elastic coefficients, $\langle M \rangle^{Hx}$ and $\left\langle \frac{\lambda}{M} \right\rangle^x \langle M \rangle^{Hx}$.
- Continuity of ε_{yy} and ε_{zz}, and the averaging of discontinuous σ_{yy} and ε_{xx} (or σ_{zz} and ε_{xx}) imply $\left\langle \frac{\lambda}{M} \right\rangle^x \langle M \rangle^{Hx}$ and two more averaged elastic coefficients: $\langle \lambda \rangle^x - \left\langle \frac{\lambda^2}{M} \right\rangle^x + \left[\left\langle \frac{\lambda}{M} \right\rangle^x \right]^2 \langle M \rangle^{Hx}$ and $\langle M \rangle^x - \left\langle \frac{\lambda^2}{M} \right\rangle^x + \left[\left\langle \frac{\lambda}{M} \right\rangle^x \right]^2 \langle M \rangle^{Hx}$.
- Considering the averaged elastic coefficients, stress- and strain-tensor components, SSRs (2.18), (2.21) and (2.22) have the same forms as SSRs for a point in a smooth medium and are consistent with the interface boundary conditions.

2.3. Elasticity matrices for interfaces perpendicular to the coordinate axes

Define

$$\begin{aligned} A^\xi &= \langle M \rangle^{H\xi} \\ B^\xi &= \left\langle \frac{\lambda}{M} \right\rangle^\xi \langle M \rangle^{H\xi} \\ C^\xi &= \langle M \rangle^\xi - \left\langle \frac{\lambda^2}{M} \right\rangle^\xi + \left[\left\langle \frac{\lambda}{M} \right\rangle^\xi \right]^2 \langle M \rangle^{H\xi} \\ D^\xi &= \langle \lambda \rangle^\xi - \left\langle \frac{\lambda^2}{M} \right\rangle^\xi + \left[\left\langle \frac{\lambda}{M} \right\rangle^\xi \right]^2 \langle M \rangle^{H\xi} \end{aligned} \tag{2.23}$$

where $\xi \in \{x, y, z\}$. Then SSRs (2.10), (2.18), (2.21) and (2.22) for a point at the interface perpendicular to the x-axis may be concisely written as

$$\begin{bmatrix} \sigma_{xx} \\ \langle \sigma_{yy} \rangle^x \\ \langle \sigma_{zz} \rangle^x \\ \sigma_{xy} \\ \langle \sigma_{yz} \rangle^x \\ \sigma_{zx} \end{bmatrix} = \begin{bmatrix} A^x & B^x & B^x & 0 & 0 & 0 \\ B^x & C^x & D^x & 0 & 0 & 0 \\ B^x & D^x & C^x & 0 & 0 & 0 \\ 0 & 0 & 0 & 2\langle \mu \rangle^{Hx} & 0 & 0 \\ 0 & 0 & 0 & 0 & 2\langle \mu \rangle^x & 0 \\ 0 & 0 & 0 & 0 & 0 & 2\langle \mu \rangle^{Hx} \end{bmatrix} \begin{bmatrix} \langle \varepsilon_{xx} \rangle^x \\ \varepsilon_{yy} \\ \varepsilon_{zz} \\ \langle \varepsilon_{xy} \rangle^x \\ \varepsilon_{yz} \\ \langle \varepsilon_{zx} \rangle^x \end{bmatrix} \tag{2.24}$$

For the interface perpendicular to the y-axis it is

$$\begin{bmatrix} \langle \sigma_{xx} \rangle^y \\ \sigma_{yy} \\ \langle \sigma_{zz} \rangle^y \\ \sigma_{xy} \\ \sigma_{yz} \\ \langle \sigma_{zx} \rangle^y \end{bmatrix} = \begin{bmatrix} C^y & B^y & D^y & 0 & 0 & 0 \\ B^y & A^y & B^y & 0 & 0 & 0 \\ D^y & B^y & C^y & 0 & 0 & 0 \\ 0 & 0 & 0 & 2\langle \mu \rangle^{Hy} & 0 & 0 \\ 0 & 0 & 0 & 0 & 2\langle \mu \rangle^{Hy} & 0 \\ 0 & 0 & 0 & 0 & 0 & 2\langle \mu \rangle^y \end{bmatrix} \begin{bmatrix} \varepsilon_{xx} \\ \langle \varepsilon_{yy} \rangle^y \\ \varepsilon_{zz} \\ \langle \varepsilon_{xy} \rangle^y \\ \langle \varepsilon_{yz} \rangle^y \\ \varepsilon_{zx} \end{bmatrix} \tag{2.25}$$

and for the interface perpendicular to the z-axis

$$\begin{bmatrix} \langle \sigma_{xx} \rangle^z \\ \langle \sigma_{yy} \rangle^z \\ \sigma_{zz} \\ \langle \sigma_{xy} \rangle^z \\ \sigma_{yz} \\ \sigma_{zx} \end{bmatrix} = \begin{bmatrix} C^z & D^z & B^z & 0 & 0 & 0 \\ D^z & C^z & B^z & 0 & 0 & 0 \\ B^z & B^z & A^z & 0 & 0 & 0 \\ 0 & 0 & 0 & 2\langle \mu \rangle^z & 0 & 0 \\ 0 & 0 & 0 & 0 & 2\langle \mu \rangle^{Hz} & 0 \\ 0 & 0 & 0 & 0 & 0 & 2\langle \mu \rangle^{Hz} \end{bmatrix} \begin{bmatrix} \varepsilon_{xx} \\ \varepsilon_{yy} \\ \langle \varepsilon_{zz} \rangle^z \\ \varepsilon_{xy} \\ \langle \varepsilon_{yz} \rangle^z \\ \langle \varepsilon_{zx} \rangle^z \end{bmatrix} \tag{2.26}$$

2.4. Elasticity matrix for an interface – interpretation

Transversely isotropic medium. Any of the matrix relations (2.24), (2.25) and (2.26) has the same form as the matrix relation for a point in a smooth medium, see Eq. (1.1), with 9 nonzero

elements (considering the symmetry of the matrix). Matrix in any of relations (2.24), (2.25) and (2.26) may be considered the elasticity matrix of an averaged medium representing contact of two materials and consistent with the boundary conditions at the welded material interface.

Matrix in Eq. (1.1) has only 2 independent nonzero elements (e.g., 2μ and $\lambda+2\mu$) because it represents an isotropic medium. Matrix for an averaged medium has 5 independent nonzero elements, e.g., A^{ξ}, B^{ξ}, C^{ξ}, $2\langle\mu\rangle^{H\xi}$ and $2\langle\mu\rangle^{\xi}$ considering that $D^{\xi}=C^{\xi}-2\langle\mu\rangle^{\xi}$. This means that the averaged medium is transversely isotropic with the axis of symmetry perpendicular to the interface.

Why is the averaged medium representing contact of two isotropic media at a planar interface transversely isotropic? SSRs for the continuous shear stress-tensor components need the harmonic average $\langle\mu\rangle^{H\xi}$ whereas the relation for the discontinuous shear stress-tensor component needs the arithmetic average $\langle\mu\rangle^{\xi}$. It is then clear that relations for the normal stress-tensor components at the interface need other independent coefficients – increasing thus the total number of coefficients: the continuous normal stress-tensor component needs 2 more independent coefficients, and the discontinuous normal stress-tensor components need, in addition to the latter 2 coefficients, also the 5th independent coefficient. The transversely isotropic medium is understandable: if it cannot be isotropic then there is no reason why it should not have the axial symmetry about the axis perpendicular to the interface.

Meaning of the harmonic averages. Consider, e.g., a planar interface perpendicular to the z-axis and a 1D problem with a wave propagating in the direction of the z-axis. Propagation of the plane P wave in any of two halfspaces is described by

$$\rho\frac{\partial^2 u_z}{\partial t^2}=\frac{\partial\sigma_{zz}}{\partial z}\quad,\quad \sigma_{zz}=\left(\lambda+2\mu\right)\frac{\partial u_z}{\partial z}=\left(\lambda+2\mu\right)\varepsilon_{zz} \tag{2.27}$$

Propagation of the plane S wave in any of two halfspaces is described by

$$\rho\frac{\partial^2 u_x}{\partial t^2}=\frac{\partial\sigma_{zx}}{\partial z}\quad,\quad \sigma_{zx}=\mu\frac{\partial u_x}{\partial z}=2\mu\varepsilon_{zx} \tag{2.28}$$

if the wave is polarized in the x direction, and by

$$\rho\frac{\partial^2 u_y}{\partial t^2}=\frac{\partial\sigma_{zy}}{\partial z}\quad,\quad \sigma_{zy}=\mu\frac{\partial u_y}{\partial z}=2\mu\varepsilon_{zy} \tag{2.29}$$

if the wave is polarized in the y direction. SSRs at the interface are then for the three cases:

$$\sigma_{zz}=\langle\lambda+2\mu\rangle^{Hz}\langle\varepsilon_{zz}\rangle^{z}\ , \tag{2.30}$$

$$\sigma_{zx} = 2\langle\mu\rangle^{Hz}\langle\varepsilon_{zx}\rangle^{z}, \tag{2.31}$$

$$\sigma_{zy} = 2\langle\mu\rangle^{Hz}\langle\varepsilon_{zy}\rangle^{z}. \tag{2.32}$$

These SSRs for the welded interface and the matrix for the averaged transversely isotropic medium representing contact of two materials and consistent with the boundary conditions at the welded material interface were presented by Moczo et al. (2002) using a matrix formalism. In this section we a) presented an alternative derivation which explicitly shows all relations between the continuous and discontinuous field quantities on one hand and the effective averaged elastic coefficients on the other hand, b) showed matrices (2.24) - (2.26) necessary for explanation of the orthorhombic averaging, c) explained structure of the elasticity matrix for the averaged transversely isotropic medium.

2.5. Planar interface in a general orientation

Assume such an interface in the Cartesian coordinate system xyz. The interface is parallel to one of the coordinate planes in some rotated system $x'y'z'$. The elasticity matrix in the rotated system has 9 non-zero elements from which 5 are independent. If we transform SSR from $x'y'z'$ into xyz, the transformed elasticity matrix has 5 independent elements (the transformation does not change the physics of the interface) but has all 21 (considering the matrix symmetry) elements non-zero. This means that all strain-tensor components are necessary for calculating each stress-tensor component at a point of the interface.

2.6. Nonplanar interface

A nonplanar smooth surface may be locally approximated by a planar interface tangential to the surface at a given point. There are two options: 1) Calculate 21 nonzero elastic coefficients for each grid point and store them in memory during the entire FD time-integration. 2) Store only 2+2 elastic coefficients (2 per medium in contact) and 2 angles (specifying orientation of an approximating tangential planar interface) for each grid point and calculate the elasticity matrix at each time step at each grid point. It is clear that we face either considerably increased memory requirement or considerably increased computing time.

2.7. A simple computational compromise – harmonic averaging

Given the situation described, Moczo et al. (2002) suggested the computational compromise: an effective grid elastic modulus at a given grid position is evaluated as the volume integral harmonic average over a grid cell centred at that grid position. Consequently, an interface between two isotropic media is represented by a harmonically averaged isotropic medium. The

advantageous aspect of the approach is that the effective grid moduli are directly applicable, e.g., to the standard velocity-stress finite-difference scheme – they do not change the structure and number of arithmetic operations in the finite-difference scheme.

2.8. Structure of the equation of motion in relation to a planar interface

Consider a planar interface between two homogeneous elastic halfspaces perpendicular to the z-axis. Fig. 2 shows the structure of the equation of motion with respect to the stress-tensor components continuous and discontinuous across the interface. The continuous stress-tensor components are in blue, the discontinuous ones are in red. The colour frames on the right-hand sides of the equations indicate parts relevant for different wavefield configurations.

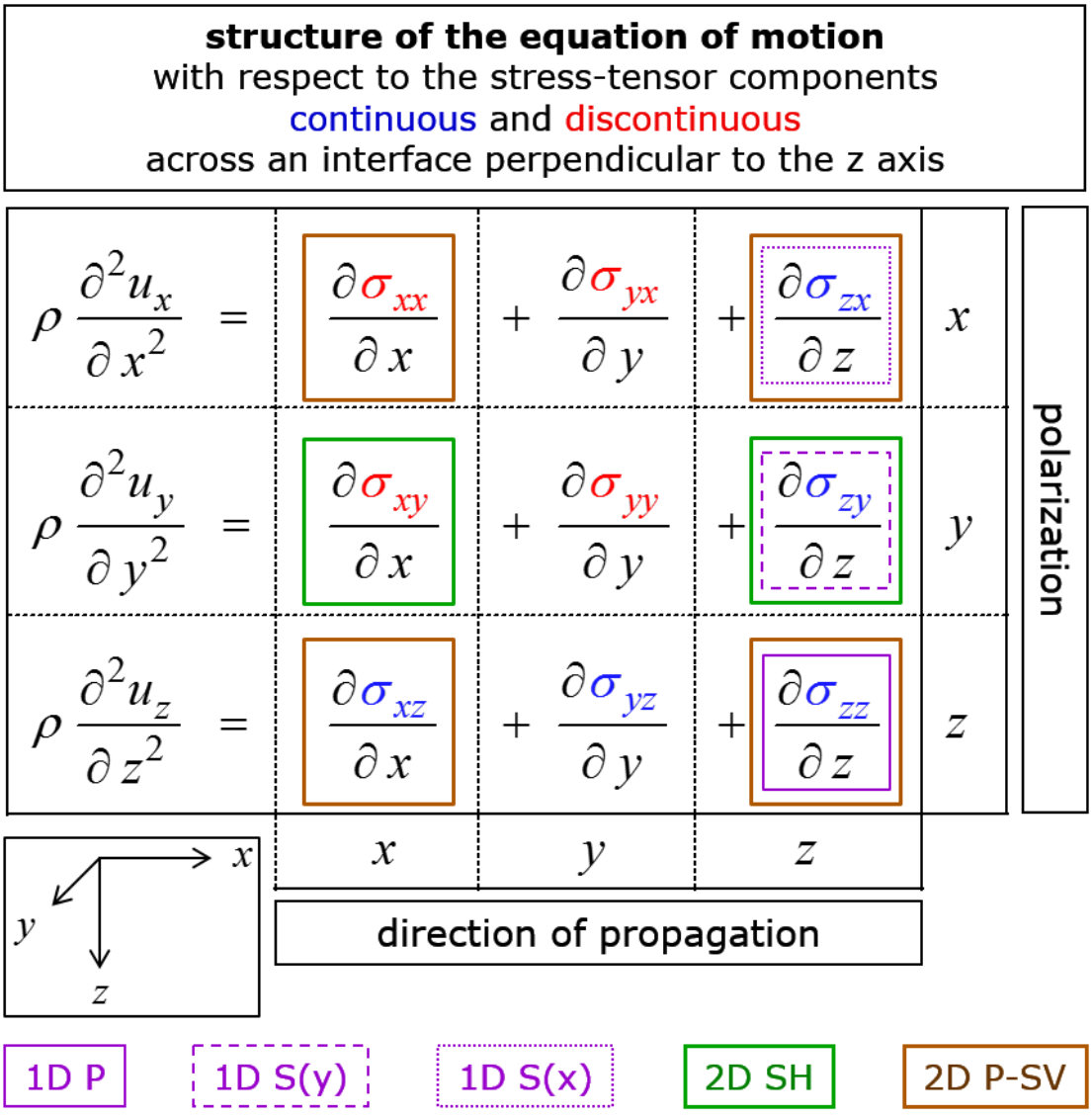

Figure 2. Structure of the equation of motion illustrating relation of the continuous and discontinuous stress-tensor components to effective medium averaging.

In any of the three simplest 1D problems with waves propagating in the $\pm z$ direction, that is, 1D P-wave, 1D S-wave polarized in the y direction and 1D S-wave polarized in the x direction (indicated by the violet frames), only one continuous stress-tensor component is involved. As shown in Section 2.4, the harmonic averaging of elastic moduli is exact in any of the three simplest 1D problems.

The 2D SH problem (green frames) involves one continuous and one discontinuous shear stress-tensor components. The harmonic averaging is exact for the continuous component whereas it is only approximate for the discontinuous one.

The 2D P-SV problem (brown frames) involves one continuous shear stress-tensor component, one continuous normal stress-tensor component and one discontinuous normal stress-tensor component. The harmonic averaging is exact for the continuous shear stress-tensor component whereas it is only approximate for the two others.

In the 3D problem the harmonic averaging is exact for two continuous shear stress-tensor components whereas it is only approximate for the four others.

Stringent numerical tests (Moczo et al. 2002, Chaljub et al. 2015) show that the harmonic averaging of moduli for all stress-tensor components is surprisingly accurate except the case when the wavefield is dominated by surface wave propagating along the contrast interface. The analysis of the stringent tests that involve dominant surface waves propagating in the horizontal direction along the strong-contrast interface (within the verification phase of the E2VP project, Chaljub et al. 2015) led us to improve the way of representing the material interface by an averaged medium. We present the new method in the following sections.

3 STRESS-STRAIN RELATION FOR A JOINT POINT OF EIGHT CUBES – SEQUENTIAL AVERAGING

Consider a joint grid point of 8 grid cells. In a simple representation of a heterogeneous medium material of each cell is homogeneous while different from materials of the other cells. It is important to find an effective material grid parameter representing heterogeneity of the medium around that grid point. There is, however, a more important reason for considering the canonical situation of a joint point of eight cubes. Consider nonplanar interfaces inside a grid cell. Then we can think of dividing the cell into homogeneous subcells and approximating the nonplanar interfaces by a staircase interfaces separating homogeneous subcells.

3.1. Shear stress-tensor components

Consider a configuration in Fig. 3: 8 homogeneous elastic infinitely large cubes in contact. The cubes may differ from each other by values of moduli. With reference to Eq. (2.8) let us write SSRs for σ_{xy} at each of 8 planar interfaces perpendicular to the horizontal Cartesian directions:

$$\begin{aligned} \sigma_{xy}^{12} &= 2\left\langle \mu \right\rangle^{Hx,12}\left\langle \varepsilon_{xy} \right\rangle^{x,12} \quad , \quad \sigma_{xy}^{34} = 2\left\langle \mu \right\rangle^{Hx,34}\left\langle \varepsilon_{xy} \right\rangle^{x,34} \\ \sigma_{xy}^{13} &= 2\left\langle \mu \right\rangle^{Hy,13}\left\langle \varepsilon_{xy} \right\rangle^{\mathrm{y},13} \quad , \quad \sigma_{xy}^{24} = 2\left\langle \mu \right\rangle^{Hy,24}\left\langle \varepsilon_{xy} \right\rangle^{\mathrm{y},24} \end{aligned} \tag{3.1}$$

and

$$\begin{aligned} \sigma_{xy}^{56} &= 2\left\langle \mu \right\rangle^{Hx,56}\left\langle \varepsilon_{xy} \right\rangle^{x,56} \quad , \quad \sigma_{xy}^{78} = 2\left\langle \mu \right\rangle^{Hx,78}\left\langle \varepsilon_{xy} \right\rangle^{x,78} \\ \sigma_{xy}^{57} &= 2\left\langle \mu \right\rangle^{Hy,57}\left\langle \varepsilon_{xy} \right\rangle^{\mathrm{y},57} \quad , \quad \sigma_{xy}^{68} = 2\left\langle \mu \right\rangle^{Hy,68}\left\langle \varepsilon_{xy} \right\rangle^{\mathrm{y},68} \end{aligned} \tag{3.2}$$

Here the superscripts indicate the interface – for example, 12 indicates the interface between cubes 1 and 2. Considering averaging along joint contact lines of the four upper and lower cubes (the four horizontal contact lines in Fig. 3), respectively, and continuity of σ_{xy} in any horizontal direction (Fig. 1), we define σ_{xy}^{-} and σ_{xy}^{+}:

$$\begin{aligned} \sigma_{xy}^{-} &\equiv \sigma_{xy}^{12} = \sigma_{xy}^{34} = \sigma_{xy}^{13} = \sigma_{xy}^{24} \\ \sigma_{xy}^{+} &\equiv \sigma_{xy}^{56} = \sigma_{xy}^{78} = \sigma_{xy}^{57} = \sigma_{xy}^{68} \end{aligned} \tag{3.3}$$

Then averaging of moduli and strains in relations (3.1) and (3.2), respectively, leads to

$$\begin{aligned} \sigma_{xy}^{-} &= 2\left\langle \mu \right\rangle^{Hxy,-}\left\langle \varepsilon_{xy} \right\rangle^{xy,-} \\ \sigma_{xy}^{+} &= 2\left\langle \mu \right\rangle^{Hxy,+}\left\langle \varepsilon_{xy} \right\rangle^{xy,+} \end{aligned} \tag{3.4}$$

where

$$\begin{aligned} \left\langle \mu \right\rangle^{Hxy,-} &= 4\left[\frac{1}{\left\langle \mu \right\rangle^{Hx,12}} + \frac{1}{\left\langle \mu \right\rangle^{Hx,34}} + \frac{1}{\left\langle \mu \right\rangle^{Hy,13}} + \frac{1}{\left\langle \mu \right\rangle^{Hy,24}} \right]^{-1} \\ \left\langle \mu \right\rangle^{Hxy,+} &= 4\left[\frac{1}{\left\langle \mu \right\rangle^{Hx,56}} + \frac{1}{\left\langle \mu \right\rangle^{Hx,78}} + \frac{1}{\left\langle \mu \right\rangle^{Hy,57}} + \frac{1}{\left\langle \mu \right\rangle^{Hy,68}} \right]^{-1} \end{aligned} \tag{3.5}$$

and

$$\begin{aligned} \left\langle \varepsilon_{xy} \right\rangle^{xy,-} &= \tfrac{1}{4}\left(\left\langle \varepsilon_{xy} \right\rangle^{x,12} + \left\langle \varepsilon_{xy} \right\rangle^{x,34} + \left\langle \varepsilon_{xy} \right\rangle^{\mathrm{y},13} + \left\langle \varepsilon_{xy} \right\rangle^{\mathrm{y},24} \right) \\ \left\langle \varepsilon_{xy} \right\rangle^{xy,+} &= \tfrac{1}{4}\left(\left\langle \varepsilon_{xy} \right\rangle^{x,56} + \left\langle \varepsilon_{xy} \right\rangle^{x,78} + \left\langle \varepsilon_{xy} \right\rangle^{\mathrm{y},57} + \left\langle \varepsilon_{xy} \right\rangle^{\mathrm{y},68} \right) \end{aligned} \tag{3.6}$$

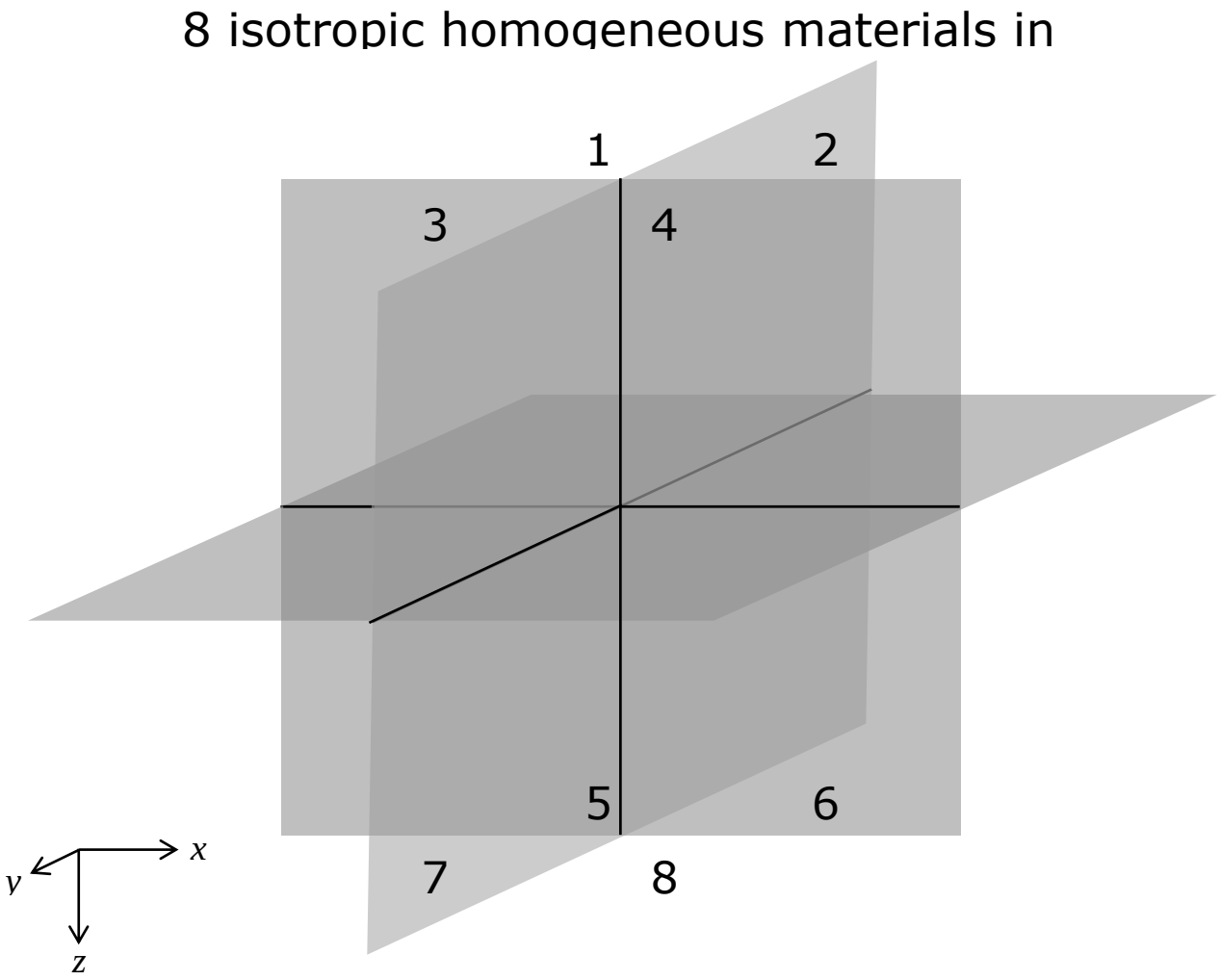

Figure 3. Illustration of interfaces separating 8 infinitely large cubes in contact. Each cube is assumed elastic and homogeneous. In general, the cubes differ from each other by values of elastic moduli and density.

Considering averaging at a joint point of eight cubes and continuity of ε_{xy} in the z direction, we define

$$\left\langle \varepsilon_{xy} \right\rangle^{xy} \equiv \left\langle \varepsilon_{xy} \right\rangle^{xy,-} = \left\langle \varepsilon_{xy} \right\rangle^{xy,+} \tag{3.7}$$

Defining also

$$\left\langle \sigma_{xy} \right\rangle^{z} \equiv \tfrac{1}{2} \left(\sigma_{xy}^{-} + \sigma_{xy}^{+} \right) \tag{3.8}$$

and

$$\left\langle \left\langle \mu \right\rangle^{Hxy} \right\rangle^{z} = \tfrac{1}{2} \left(\left\langle \mu \right\rangle^{Hxy,-} + \left\langle \mu \right\rangle^{Hxy,+} \right) \tag{3.9}$$

we finally obtain from (3.4) SSR for the joint point of eight cubes:

$$\left\langle \sigma_{xy} \right\rangle^{z} = 2\left\langle \left\langle \mu \right\rangle^{Hxy} \right\rangle^{z} \left\langle \varepsilon_{xy} \right\rangle^{xy} \tag{3.10}$$

We have obtained this relation by averaging first in the horizontal directions x and y, and then averaging in the z direction. We may try also the opposite way: averaging first in the z direction and then in the horizontal directions.

With reference to Eq. (2.3), consider therefore, instead of Eqs. (3.1) and (3.2), the following relations for the four interfaces perpendicular to the z axis:

$$\begin{aligned} \left\langle \sigma_{xy} \right\rangle^{z,15} &= 2\left\langle \mu \right\rangle^{z,15} \varepsilon_{xy}^{15} \quad , \quad \left\langle \sigma_{xy} \right\rangle^{z,26} = 2\left\langle \mu \right\rangle^{z,26} \varepsilon_{xy}^{26} \\ \left\langle \sigma_{xy} \right\rangle^{z,37} &= 2\left\langle \mu \right\rangle^{z,37} \varepsilon_{xy}^{37} \quad , \quad \left\langle \sigma_{xy} \right\rangle^{z,48} = 2\left\langle \mu \right\rangle^{z,48} \varepsilon_{xy}^{48} \end{aligned} \tag{3.11}$$

Consider now interfaces perpendicular to the x and y axes. Because σ_{xy} is continuous in both x and y directions, we may define

$$\left\langle \sigma_{xy} \right\rangle^{z} \equiv \left\langle \sigma_{xy} \right\rangle^{z,15} = \left\langle \sigma_{xy} \right\rangle^{z,26} = \left\langle \sigma_{xy} \right\rangle^{z,37} = \left\langle \sigma_{xy} \right\rangle^{z,48} \tag{3.12}$$

Then averaging of moduli and strains in relations (3.11) in the x and y directions, respectively, leads to

$$\begin{aligned} \left\langle \sigma_{xy} \right\rangle^{z} &= 4\left[\frac{1}{\left\langle \mu \right\rangle^{z,15}} + \frac{1}{\left\langle \mu \right\rangle^{z,26}} \right]^{-1} \frac{1}{2}\left(\varepsilon_{xy}^{15} + \varepsilon_{xy}^{26} \right) \\ \left\langle \sigma_{xy} \right\rangle^{z} &= 4\left[\frac{1}{\left\langle \mu \right\rangle^{z,37}} + \frac{1}{\left\langle \mu \right\rangle^{z,48}} \right]^{-1} \frac{1}{2}\left(\varepsilon_{xy}^{37} + \varepsilon_{xy}^{48} \right) \end{aligned} \tag{3.13}$$

and

$$\begin{aligned} \left\langle \sigma_{xy} \right\rangle^{z} &= 4\left[\frac{1}{\left\langle \mu \right\rangle^{z,15}} + \frac{1}{\left\langle \mu \right\rangle^{z,37}} \right]^{-1} \frac{1}{2}\left(\varepsilon_{xy}^{15} + \varepsilon_{xy}^{37} \right) \\ \left\langle \sigma_{xy} \right\rangle^{z} &= 4\left[\frac{1}{\left\langle \mu \right\rangle^{z,26}} + \frac{1}{\left\langle \mu \right\rangle^{z,48}} \right]^{-1} \frac{1}{2}\left(\varepsilon_{xy}^{26} + \varepsilon_{xy}^{48} \right) \end{aligned} \tag{3.14}$$

Summation of the four relations (3.13) and (3.14) eventually leads to

$$\left\langle \sigma_{xy} \right\rangle^{z} = 2\left\langle \left\langle \mu \right\rangle^{z} \right\rangle^{Hxy} \left\langle \varepsilon_{xy} \right\rangle^{xy} \tag{3.15}$$

where $\left\langle \left\langle \mu \right\rangle^{z} \right\rangle^{Hxy}$ denotes the harmonic average of the four harmonic averages in relations (3.13) and (3.14), and $\left\langle \varepsilon_{xy} \right\rangle^{xy}$ denotes the arithmetic average of the four arithmetic averages of strain in relations (3.13) and (3.14).

It is obvious from comparison of relations (3.10) and (3.15) that the order of averaging leads to relations with differently averaged moduli. At the same time, we immediately see two common features of both averages, $\left\langle \mu^{Hxy} \right\rangle^{z}$ and $\left\langle \left\langle \mu \right\rangle^{z} \right\rangle^{Hxy}$: 1. continuity of σ_{xy} in the x and y directions implies the harmonic averaging in both directions, 2. discontinuity of σ_{xy} in the z direction implies the arithmetic averaging in that direction. Both obtained SSRs are just different approximations and it is difficult to say which one is better. We may use, however, an additional criterion to choose one of them. Consider, e.g., one of cubes representing a liquid or vacuum. Then the corresponding harmonic average $\left\langle \mu \right\rangle^{Hxy}$ would give a zero average value for the four cubes. This would be not the case with the arithmetic averaging applied first. Consequently we choose relation (3.15). In summary, all SSRs are

$$\begin{aligned} \left\langle \sigma_{xy} \right\rangle^{z} &= 2\left\langle \left\langle \mu \right\rangle^{z} \right\rangle^{Hxy} \left\langle \varepsilon_{xy} \right\rangle^{xy} \\ \left\langle \sigma_{yz} \right\rangle^{x} &= 2\left\langle \left\langle \mu \right\rangle^{x} \right\rangle^{Hyz} \left\langle \varepsilon_{yz} \right\rangle^{yz} \\ \left\langle \sigma_{zx} \right\rangle^{y} &= 2\left\langle \left\langle \mu \right\rangle^{y} \right\rangle^{Hzx} \left\langle \varepsilon_{zx} \right\rangle^{zx} \end{aligned} \tag{3.16}$$

Important property of the averaged moduli. Consider a 3D grid cell and evaluation of the average moduli over the volume of the cell. Assume, e.g., that the grid cell contains only one interface perpendicular to the x axis. Then relations (3.16) reduce to

$$\begin{aligned} \sigma_{xy} &= 2\left\langle \mu \right\rangle^{Hx} \left\langle \varepsilon_{xy} \right\rangle^{x} \\ \left\langle \sigma_{yz} \right\rangle^{x} &= 2\left\langle \mu \right\rangle^{x} \quad \varepsilon_{yz} \\ \sigma_{zx} &= 2\left\langle \mu \right\rangle^{Hx} \left\langle \varepsilon_{zx} \right\rangle^{x} \end{aligned} \tag{3.17}$$

that is to SSRs for the transversely isotropic medium – see Eq. (2.24). Analogously, relations (3.16) reduce to relations for the transversely isotropic medium with the axis of symmetry parallel with the y or z axis for an interface perpendicular to the y or z axis, respectively.

3.2. Normal Stress-tensor components

Formal averaging of the normal stress-tensor components at the joint point of 8 homogeneous cubes (Fig. 3) is considerably more complicated and rather lengthy. Therefore we just outline essential aspects.

We may start, e.g., with SSRs (2.24) at the interfaces perpendicular to the x axis and average them first at the interfaces perpendicular to the y axis. It is the simplest to start with SSR

for σ_{yy}, that is, $\langle\sigma_{yy}\rangle^x\left(\langle\varepsilon_{xx}\rangle^x, \varepsilon_{yy}, \varepsilon_{zz}\right)$. Because only ε_{yy} from the four field quantities in the relation is discontinuous across the interface perpendicular to the y axis, the averaging can be achieved by averaging the relation $\varepsilon_{yy}\left(\langle\varepsilon_{xx}\rangle^x, \varepsilon_{zz}, \langle\sigma_{yy}\rangle^x\right)$. The result of the averaging is $\langle\varepsilon_{yy}\rangle^y\left(\langle\varepsilon_{xx}\rangle^x, \varepsilon_{zz}, \langle\sigma_{yy}\rangle^x\right)$ from which we obtain the sought SSR for $\langle\sigma_{yy}\rangle^x$ at the interface perpendicular to the y axis: $\langle\sigma_{yy}\rangle^x\left(\langle\varepsilon_{xx}\rangle^x, \langle\varepsilon_{yy}\rangle^y, \varepsilon_{zz}\right)$.

We may continue with σ_{xx}. In SSR for σ_{xx} at the interface perpendicular to the x-axis, $\sigma_{xx}\left(\langle\varepsilon_{xx}\rangle^x, \varepsilon_{yy}, \varepsilon_{zz}\right)$, two quantities are discontinuous across the interface perpendicular to the y axis: σ_{xx} and ε_{yy}. Therefore, before we average σ_{xx} at the interface, we must express ε_{yy} from SSR $\langle\sigma_{yy}\rangle^x\left(\langle\varepsilon_{xx}\rangle^x, \varepsilon_{yy}, \varepsilon_{zz}\right)$ at the interface perpendicular to the x-axis. We obtain $\sigma_{xx}\left(\langle\varepsilon_{xx}\rangle^x, \varepsilon_{zz}, \langle\sigma_{yy}\rangle^x\right)$. Because $\langle\varepsilon_{xx}\rangle^x, \varepsilon_{zz}, \langle\sigma_{yy}\rangle^x$ are continuous across the interface perpendicular to the y-axis, we may average σ_{xx}. The result of averaging is $\langle\sigma_{xx}\rangle^y\left(\langle\varepsilon_{xx}\rangle^x, \varepsilon_{zz}, \langle\sigma_{yy}\rangle^x\right)$. In this relation we express $\langle\sigma_{yy}\rangle^x$ from relation for σ_{yy} at the interface perpendicular to the y-axis, $\langle\sigma_{yy}\rangle^x\left(\langle\varepsilon_{xx}\rangle^x, \langle\varepsilon_{yy}\rangle^y, \varepsilon_{zz}\right)$, and eventually obtain SSR at the interface perpendicular to the y axis: $\langle\sigma_{xx}\rangle^y\left(\langle\varepsilon_{xx}\rangle^x, \langle\varepsilon_{yy}\rangle^y, \varepsilon_{zz}\right)$.

Analogously we could continue with σ_{zz}. Having SSRs for the normal stress-tensor components averaged across the interfaces perpendicular to the x and y-axes, we could then continue with averaging across the interface perpendicular to the z axis.

It is obvious, however, that we could start the averaging procedure from SSRs (2.25) for the interfaces perpendicular to the y-axis, continue with averaging across the interfaces perpendicular to the z axis and finish with averaging across the interfaces perpendicular to the x axis. Eventually and alternatively, the order of averaging might be $z \to x \to y$.

The problem, indicated already by averaging the shear stress-tensor components, is that the three different sequences of averaging (that is, $x \to y \to z$, $y \to z \to x$ and $z \to x \to y$) give three different averaged moduli in SSRs for the joint point of 8 cubes. This is not acceptable because the averaged medium should not depend on the order of averaging. The three different

results are consequence of the fact that such averaging is not rigorous and justified. It is just approximate.

4 DECISION ON AVERAGING IN THE CELL VOLUME: THE ORTHORHOMBIC MEDIUM

It is obvious that we are facing two problems: 1. We do not want to have 21 nonzero coefficients in the elasticity matrix (see Sections 2.5 and 2.6). That would considerably decrease computational efficiency. 2. The sequential averaging (Sections 3.1 and 3.2) is not applicable. In this situation we have to decide how to average medium in order to obtain sufficiently accurate and computationally efficient representation of a material interface.

It is reasonable to impose two requirements in this decision-making:

1st. Keeping the number of nonzero coefficients in the elasticity matrix the same as for the isotropic or transversely isotropic media, that is, 9 (considering the matrix symmetry). This means that the averaged medium would neither change the structure of calculating stress-tensor components nor increase the number of arithmetic operations.

2nd. If a grid cell contains a planar interface (between two homogeneous materials) perpendicular to the ξ axis, then the averaged medium in the cell is the transversely isotropic medium with axis of symmetry parallel to the ξ axis.

Consequently, the elasticity matrix should have the following general form:

$$\begin{bmatrix} \Pi_x & \lambda_{xy} & \lambda_{zx} & 0 & 0 & 0 \\ \lambda_{xy} & \Pi_y & \lambda_{yz} & 0 & 0 & 0 \\ \lambda_{zx} & \lambda_{yz} & \Pi_z & 0 & 0 & 0 \\ 0 & 0 & 0 & 2\mu_{xy} & 0 & 0 \\ 0 & 0 & 0 & 0 & 2\mu_{yz} & 0 \\ 0 & 0 & 0 & 0 & 0 & 2\mu_{zx} \end{bmatrix} \tag{4.1}$$

As we explained in Section 3.1 we can take Eq. (3.16) for the shear stress-tensor components:

$$\begin{aligned} \mu_{xy} &= \left\langle \langle \mu \rangle^{z} \right\rangle^{Hxy} \\ \mu_{yz} &= \left\langle \langle \mu \rangle^{x} \right\rangle^{Hyz} \\ \mu_{zx} &= \left\langle \langle \mu \rangle^{y} \right\rangle^{Hzx} \end{aligned} \tag{4.2}$$

Figure 4. Coefficients for the normal stress-tensor components in the transversely isotropic media representing the planar interfaces perpendicular to the coordinate axes. Colours help to distinguish different averaged moduli.

With the normal stress-tensor components it is more complicated. For finding a solution, it is instructive and helpful to see the coefficients for transversely isotropic media representing the planar interfaces perpendicular to the coordinate axes at once. We show them in Fig. 4. According to the 2nd requirement, e.g., Π_x has to give $\langle M \rangle^{Hx}$ or $\left\langle M - \frac{\lambda^2}{M} \right\rangle^{y} + \left[\left\langle \frac{\lambda}{M} \right\rangle^{y} \right]^2 \langle M \rangle^{Hy}$ or $\left\langle M - \frac{\lambda^2}{M} \right\rangle^{z} + \left[\left\langle \frac{\lambda}{M} \right\rangle^{z} \right]^2 \langle M \rangle^{Hz}$ if the grid cell contains interface perpendicular to the x or y or z-axis, respectively. Analogous requirements apply to the other Π_ξ and $\lambda_{\xi\eta}$ coefficients. All these requirements are met by the following averages:

$$\begin{aligned}
\Pi_x &= \left\langle \left\langle M - \frac{\lambda^2}{M} \right\rangle^{yz} + \left[\left\langle \frac{\lambda}{M} \right\rangle^{yz} \right]^2 \langle M \rangle^{Hyz} \right\rangle^{Hx} \\
\Pi_y &= \left\langle \left\langle M - \frac{\lambda^2}{M} \right\rangle^{zx} + \left[\left\langle \frac{\lambda}{M} \right\rangle^{zx} \right]^2 \langle M \rangle^{Hzx} \right\rangle^{Hy} \qquad (4.3) \\
\Pi_z &= \left\langle \left\langle M - \frac{\lambda^2}{M} \right\rangle^{xy} + \left[\left\langle \frac{\lambda}{M} \right\rangle^{xy} \right]^2 \langle M \rangle^{Hxy} \right\rangle^{Hz}
\end{aligned}$$

and

$$\begin{aligned}
\lambda_{xy} &= \left\langle \left\langle M - \frac{\lambda^2}{M} \right\rangle^{z} + \left[\left\langle \frac{\lambda}{M} \right\rangle^{z} \right]^2 \langle M \rangle^{Hz} \right\rangle^{Hxy} \\
&\quad \left\langle \frac{\left\langle \lambda - \frac{\lambda^2}{M} \right\rangle^{z} + \left[\left\langle \frac{\lambda}{M} \right\rangle^{z} \right]^2 \langle M \rangle^{Hz}}{\left\langle M - \frac{\lambda^2}{M} \right\rangle^{z} + \left[\left\langle \frac{\lambda}{M} \right\rangle^{z} \right]^2 \langle M \rangle^{Hz}} \right\rangle^{xy} \qquad (4.4) \\
\lambda_{yz} &= \left\langle \left\langle M - \frac{\lambda^2}{M} \right\rangle^{x} + \left[\left\langle \frac{\lambda}{M} \right\rangle^{x} \right]^2 \langle M \rangle^{Hx} \right\rangle^{Hyz} \\
&\quad \left\langle \frac{\left\langle \lambda - \frac{\lambda^2}{M} \right\rangle^{x} + \left[\left\langle \frac{\lambda}{M} \right\rangle^{x} \right]^2 \langle M \rangle^{Hx}}{\left\langle M - \frac{\lambda^2}{M} \right\rangle^{x} + \left[\left\langle \frac{\lambda}{M} \right\rangle^{x} \right]^2 \langle M \rangle^{Hx}} \right\rangle^{yz} \qquad (4.5)
\end{aligned}$$

$$\lambda_{zx} = \left\langle \left\langle M - \frac{\lambda^2}{M} \right\rangle^y + \left[\left\langle \frac{\lambda}{M} \right\rangle^y \right]^2 \langle M \rangle^{Hy} \right\rangle^{Hzx} \left\langle \frac{\left\langle \lambda - \frac{\lambda^2}{M} \right\rangle^y + \left[\left\langle \frac{\lambda}{M} \right\rangle^y \right]^2 \langle M \rangle^{Hy}}{\left\langle M - \frac{\lambda^2}{M} \right\rangle^y + \left[\left\langle \frac{\lambda}{M} \right\rangle^y \right]^2 \langle M \rangle^{Hy}} \right\rangle^{zx} \tag{4.6}$$

Each average applies to a volume of the grid cell $h \times h \times h$ centred at a position of the stress-tensor component. We see that the 9 coefficients are independent. This means that the averaged medium has an orthorhombic anisotropy with three axes of symmetry that are identical with coordinate axes.

5 NUMERICAL VERIFICATION

Because the developed discrete representation is approximate it is necessary to test it numerically by comparing the finite-difference (FD) seismograms with seismograms obtained using independent verified methods. Whereas for a 1D model it is possible to use the very accurate semianalytical discrete-wavenumber method (DWM), for 2D and 3D models we can only use an approximate but sufficiently accurate numerical method. We have chosen the spectral-element method (SEM). Tests for 1D and 2D models were performed and published – we will just briefly mention the substantial aspects. In this article we present 3D tests.

5.1. 1D models

Moczo et al. (2014) and Chaljub et al. (2015) presented numerical tests for a set of canonical 1D models. One model, denoted as Can2, consists of three horizontal homogeneous elastic isotropic layers over halfspace. The model represents the vertical profile beneath the TST seismic station in the Mygdonian basin near Thessaloniki in Greece. A 3D wavefield is generated by a single vertical force at the free surface and a point double-couple (DC) source in the halfspace – in order to include both intensive surface and body waves. The simulations are performed for frequencies up to 4 Hz. The other model, Can3, is a modification of Can2: there are vertical constant gradients of material parameters in the layers. The reference solutions are obtained using two DWN codes - Axitra (Bouchon 1981, Coutant 1989) for the DC source and the code developed by Hisada (1994, 1995) for the surface force. The FD seismograms are obtained for four alternative representations: LOC – local (point) values of the elastic moduli and density, ARI – volume arithmetic averages of moduli and volume arithmetic averages of density

evaluated using numerical integration over a grid cell centred at the grid position of the modulus or density, HAR – volume harmonic averages of moduli and volume arithmetic averages of density, and ORT – volume effective coefficients corresponding to the orthorhombic averaged medium. The level of agreement between the FD and DWN seismograms in phase and amplitude is quantified using the time-frequency phase and envelope goodness-of-fit (GOF) criteria (Kristekova et al. 2009). The orthorhombic representation yields the best results.

5.2. 2D model

Testing the orthorhombic representation in a 2D model is much more complicated. Moczo et al. (2014) and Chaljub et al. (2015) used a 2D model representing a simplified NS profile of the Mygdonian basin going through the TST seismic station and 3D wavefield due the point DC source in the halfspace. They compared the HAR and ORT FD seismograms with seismograms simulated by the Florent De Martin's SEM code efispec (De Martin 2011). Accuracy of the SEM solution is strongly determined by discretization of the wedge-type Northern margin of the basin. Florent De Martin developed an extremely fine SEM mesh following all material interfaces (though obviously relative, the minimum size of the element is only 0.5 m in simulation up to 4 Hz and minimum S-wave speed of 200 m/s). Consequently, the SEM simulation was computationally extremely demanding. It provided, however, the best feasible reference solution for testing the orthorhombic discretization. The ORT representation yields FD seismograms that are in excellent agreement with the SEM reference seismograms. The HAR representation yields FD seismograms that are in excellent agreement with the SEM seismograms except at receivers where the motion is dominated by surface waves propagating along the horizontal interfaces.

5.3. 3D model

The approach applied in testing the orthorhombic representation in 2D was not feasible in 3D due to extreme computational time and memory requirements. In order to obtain a sufficiently accurate reference SEM seismograms, we developed a special model. In the available realistic 3D model of the Mygdonian basin we modified geometry of material interfaces so that the element faces can exactly follow interfaces. This means that the SEM simulation exactly accounts for the geometry of material interfaces and consequently the SEM seismograms are adequately accurate. Fig. 5 illustrates the SEM mesh. Contact of elements with different colours is a material interface. There are 5 interfaces in the figure showing a detail of the basin edge.

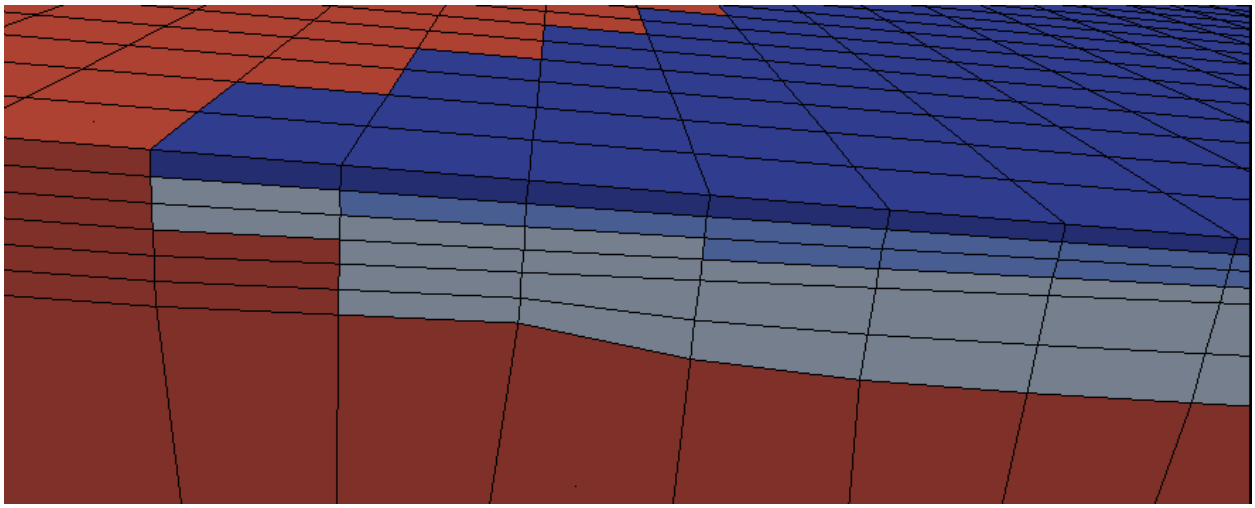

Figure 5. Illustrative detail of the reference SEM model. Different colours represent different homogeneous materials. Element faces exactly follow interfaces. This specific feature makes it possible for SEM to produce sufficiently accurate seismograms. Exactly the same model is considered in the FD simulation.

The original model of the Mygdonian basin is shown in Fig. 6. The upper left panel shows margins of the sedimentary basin at the flat free surface, four horizontal profiles of receivers at the free surface and position of the vertical profile of receivers in the central part of the basin. The FD and SEM seismograms are compared along the receiver profiles.

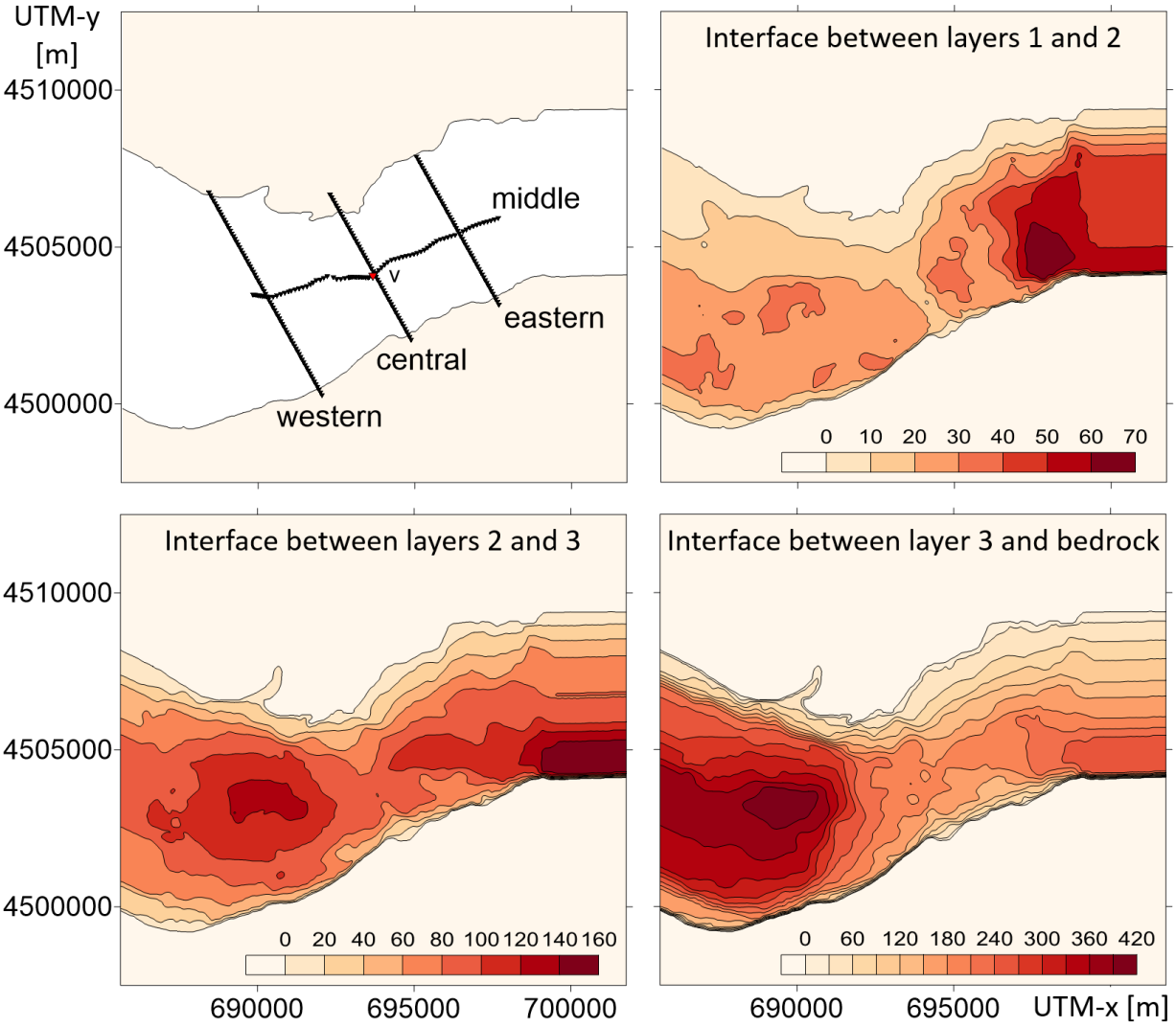

Figure 6. Geometry of the original 3D model of the Mygdonian basin. Upper left panel: margins of the sedimentary basin at the flat free surface, four horizontal profiles of receivers at the free surface and position of the vertical profile of receivers (v) in the central part of the basin. Upper right: interface between the uppermost and middle sedimentary layers. Lower left: interface between the middle and bottom sedimentary layers. Lower right: interface between the bottom sedimentary layer and bedrock.

Material parameters of the model are shown in Fig. 7.

Layer	V_S	V_P	ρ
	(m/s)	(m/s)	(kg/m^3)
1	200	1500	2100
2	350	1800	2200
3	650	2500	2200
Bedrock	2600	4500	2600

Figure 7. Material parameters of the 3D model of the Mygdonian basin.

The wavefield is generated by a DC point source located at a depth of 5 km. The source time function is shown in Fig. 8. The slip-rate time function is defined as a low-pass filtered gaussian pulse. The slip is obtained by integration of the slip rate.

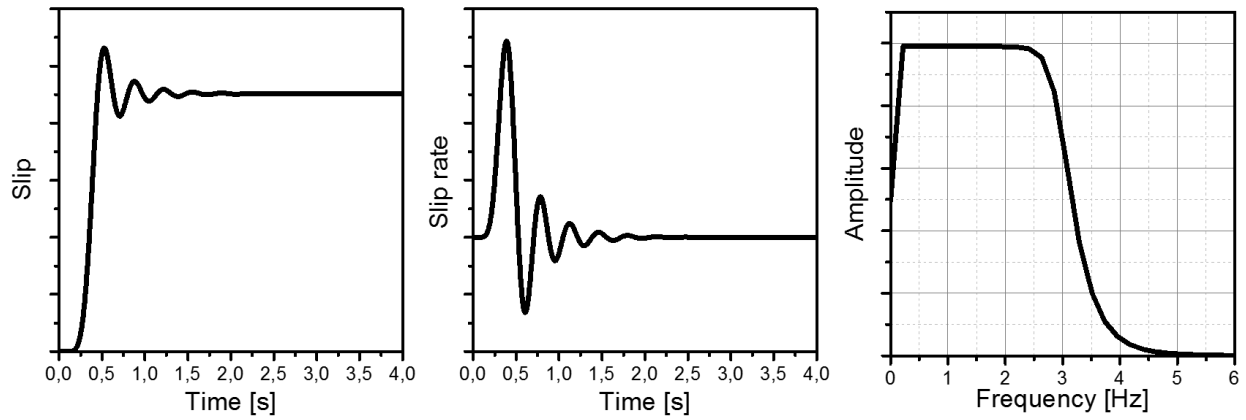

Figure 8. The source time function. Left: slip, centre: slip rate, right: Fourier amplitude spectrum of the slip rate.

The reference SEM seismograms were computed using the SPECFEM3D code developed by Komatitsch and Tromp (e.g., Komatitsch and Tromp 1999, Tromp et al. 2008, Peter et al. 2011). The FDM seismograms were computed using the FDSim3D code (Kristek & Moczo 2014, Moczo et al. 2014). Figs. 9 and 10 summarize the SEM and FDM computational parameters.

computational domain	16.14 km x 29.31 km x 7.86 km		
number of elements	1 751 040		
polynomial degree	N=4 (5 GLL points per direction)		
number of points (each counted once)	115 605 072		
		vertical	horizontal
(upper) fine mesh	element size	2.5-7.5 m	50 m
	average grid spacing	0.62-1.87 m	12.5 m
	minimum grid spacing	0.43-1.30 m	8.63 m
(lower) coarse mesh	element size	860 m	200 m
	average grid spacing	215 m	50 m
	minimum grid spacing	148.50 m	34.53 m
time step	0.0001 s		
time window	30 s		
note: minimum grid spacing = 0.691 % of average gridsize for N=4			

Figure 9. Computational parameters of the SEM simulation. GLL means Gauss-Lobatto-Legendre.

		FDM 10 m	FDM 7 m
fine grid	size	1585 x 1475 x 59	2113 x 2113 x 84
	grid spacing	10 m	7 m
	PML zone	55 grid planes	55 grid planes
coarse grid	size	145 x 135 x 140	193 x 193 x 200
	grid spacing	110 m	77 m
	PML zone	5 grid planes	5 grid planes
time step		0.001 s	0.0007 s
time window		30 s	30 s

Figure 10. Computational parameters of the FDM simulations with the 10-m and 7-m grid spacings.

We calculated the ORT FD seismograms using two spatially discontinuous grids. The size of the fine-grid spacing is 10 m in the first grid and 7 m in the second grid. As in the 1D and 2D models, it is reasonable to compare the ORT FD seismograms not only with the reference SEM seismograms but also with HAR FD seismograms. The HAR seismograms were also calculated using the two discontinuous grids. Fig. 11 shows the envelope and phase GOFs (goodness-of-fit) between the reference SEM seismograms and FDM seismograms along the western, central and eastern receiver profiles. Each curve represents GOF between the SEM and respective FD seismograms. GOFs are calculated for the entire 30-s window in the frequency range [0.1, 5] Hz from the arithmetic average of the single-valued misfits evaluated separately for each component (Kristekova et al. 2009). Fig. 12 shows the envelope and phase GOFs for the middle and vertical receiver profiles. Recall that GOF=10 means the perfect agreement.

Overall for a given discrete representation (ORT or HAR) the GOF values for the 7-m grid spacing are larger than the GOF values for the 10-m grid spacing. This means that, for a given discrete representation, the FD seismograms for the smaller size of the grid spacing are closer to the SEM seismograms compared to the FD seismograms for the larger size of the grid spacing. This is what one expects.

The more important is comparison of the two discrete representations. Overall for a given spatial grid the phase GOF values for the ORT discrete representation are significantly larger than the phase GOF values for the HAR representation. In other words, the ORT FD seismograms are significantly closer in phase to the SEM seismograms than the HAR FD

seismograms are. The improvement in terms of the envelope GOFs due to the ORT representation compared to the HAR representation is considerable although not as significant as in the phase GOFs.

It is also interesting and important to compare the HAR 7-m FD seismograms with the ORT 10-m FD seismograms. Despite the larger grid spacing the ORT 10-m FD seismograms are significantly more accurate in phase than the HAR 7-m FD seismograms. They are comparably-to-slightly-more accurate in envelope.

Fig. 13 shows seismograms for receiver 166 at the middle profile. The phase GOF values between the four FD seismograms and the reference SEM seismogram at this receiver range approximately from 3.5 to 9. Although we look at just one receiver, the relatively large range of the GOF values makes it possible to reasonably illustrate differences in seismograms corresponding to different GOF values.

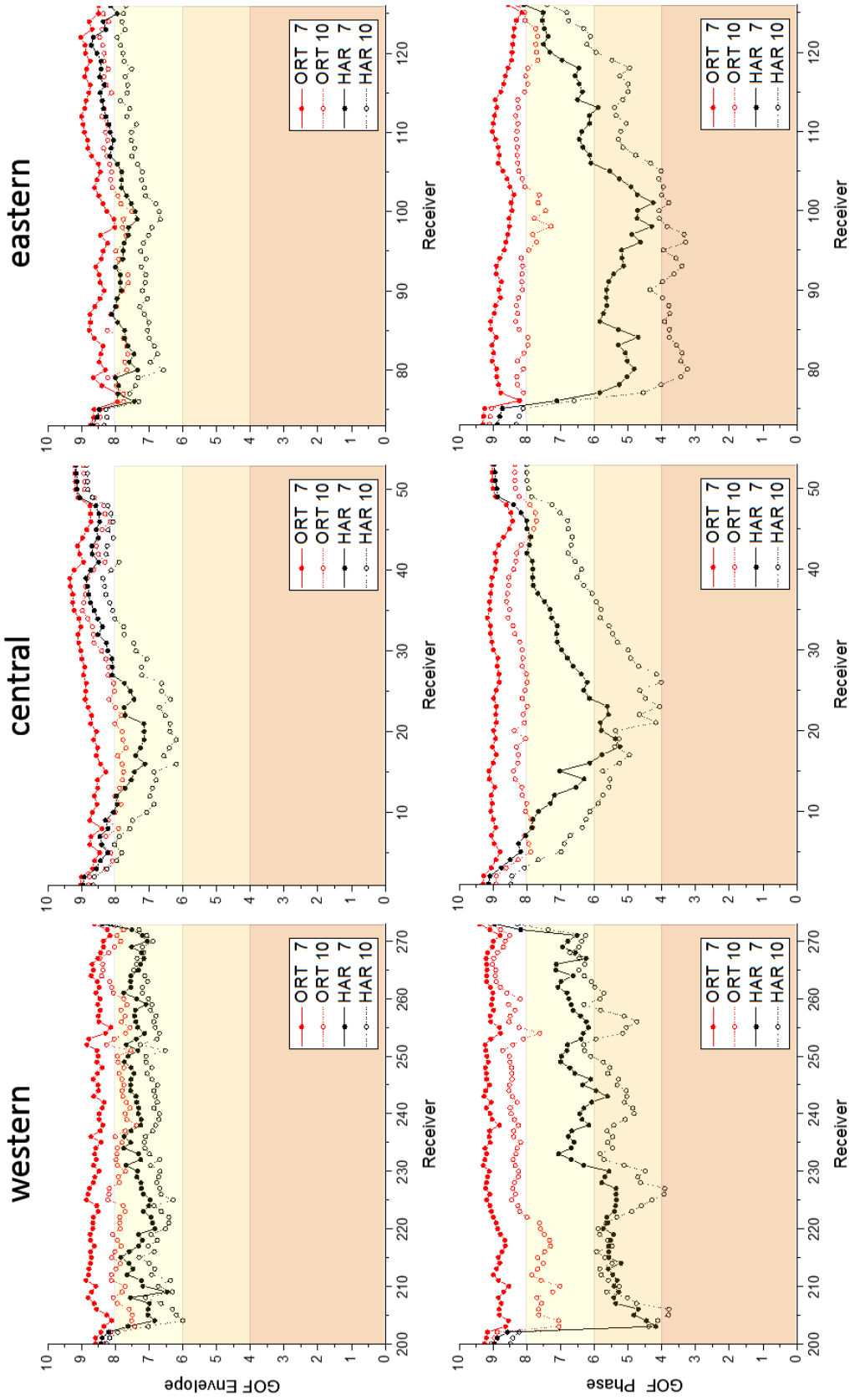

Figure 11. The envelope and phase GOFs (goodness-of-fit) between the reference SEM seismograms and FDM seismograms along the western, central and eastern receiver profiles. The FDM seismograms were obtained using the orthorhombic (ORT) and harmonic (HAR) averaging for the 10-m and 7-m grid spacings.

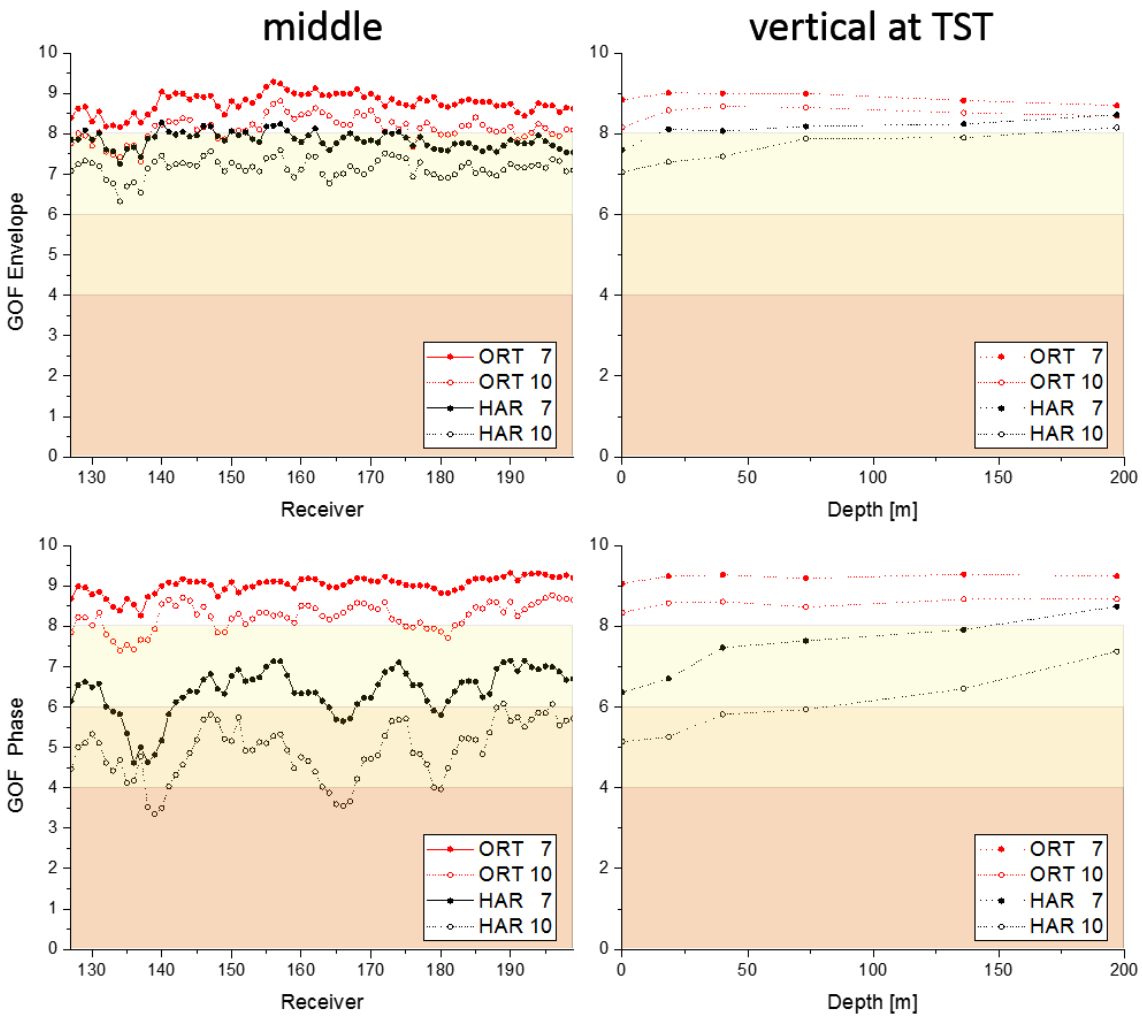

Figure 12. The envelope and phase GOFs (goodness-of-fit) between the reference SEM seismograms and FDM seismograms along the middle profile and vertical profile. The FDM seismograms were obtained using the orthorhombic (ORT) and harmonic (HAR) averaging for the 10-m and 7-m grid spacings.

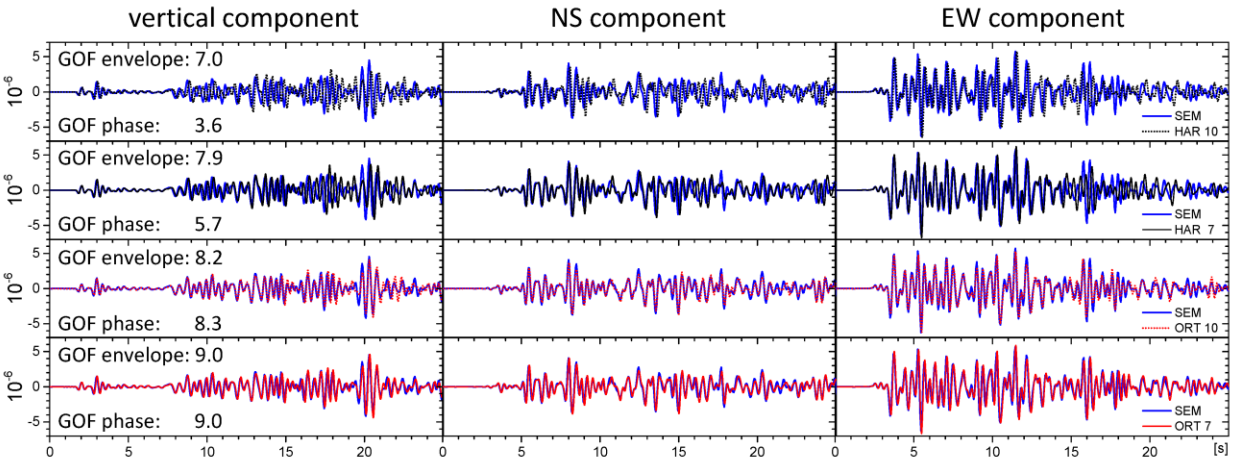

Figure 13. Comparison of the four FD seismograms with the reference SEM seismogram for receiver 166 at the middle profile.

6 ACCURACY AND EFFICIENCY OF THE ORTHORHOMBIC REPRESENTATION AND FINITE-DIFFERENCE MODELLING

Recall Fig. 5 illustrating an important aspect of the SEM modelling. It is natural to cover the spatial computational domain with elements of different shapes and sizes. Consequently, it is possible for SEM to follow geometry of a material interface piece-wise by element faces. This is significant for accuracy of the SEM modelling but, at the same time, can considerably increase the number of elements e.g. in the case of a wedge of a sedimentary layer. In fact, this aspect led to the computationally very much demanding 2D model developed by Florent De Martin (Section 5.2) as well as to the necessity to adjust geometry of material interfaces in the reference 3D model of the Mygdonian basin for verification in this study. Obviously, the smaller size of an element, the smaller size of the time step and, consequently, the larger number of time levels to be computed.

The FD modelling is computationally most efficient on the uniform grid and in the heterogeneous formulation. The latter means that one FD scheme is applied to all grid points except those forming a border of the grid. The use of one scheme everywhere means that both smooth and discontinuous heterogeneity has to be accounted for by effective values of moduli and density at respective grid points. An effective grid modulus is evaluated numerically as a volume orthorhombic average in a grid cell centred at the grid position of the corresponding stress-tensor component. An effective density is evaluated numerically as a volume arithmetic average in a grid cell centred at the grid position of the corresponding particle-velocity component. The geometry as well as material properties on both sides of the interface are accounted for by the effective grid moduli and densities. In other words, in a chosen spatial grid, geometry of an interface may be arbitrary. For a given frequency range, change of interface geometry neither requires a new grid, nor changed computational demands. This is the significant advantage of the FD modelling. We illustrate this advantage in Fig. 14.

Note that the size of the FD grid cell should not be directly compared with the size of the SEM element. A SEM element for a given polynomial degree includes certain number of the GLL integration points per direction. For example, in the reference SEM calculation the polynomial degree is 4 and thus the number of GLL points per direction is 5. Therefore, for computational efficiency it is reasonable to compare the total number of the FD grid points with the total number of the GLL points. Usually, in the case of local surface sedimentary structures with flat free surface, the application of a FD discontinuous spatial grid and effective grid moduli is computationally more efficient than the application of SEM for a given frequency range and

level of accuracy. The SEM computational requirements should be decreased if the orthorhombic representation is applied and interfaces are not followed by element faces.

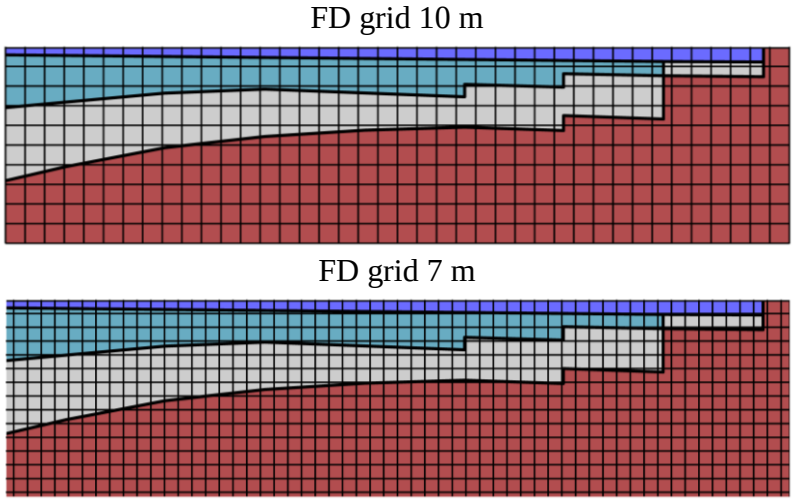

Figure 14. Illustration of the FD grid and material interfaces – a detail of one vertical grid plane crossing the sediment layers in the Mygdonian basin model. Assuming a proper evaluation of the effective grid moduli and densities at grid points there is no need for the grid to be conformable with interfaces.

7 CONCLUSIONS

We presented derivation of the stress-strain relation for a point at a planar interface between two homogeneous halfspaces. The derivation is an alternative to the matrix derivation by Moczo et al. (2002). Contrary to that the presented derivation makes it possible to interpret the obtained average elastic moduli with respect to continuous and discontinuous stress- and strain-tensor components.

We showed that the approach applicable to the planar interface is not applicable to the joint point of 8 homogeneous infinitely large cubes. The average moduli depend on the sequence of averaging (that is, $x \to y \to z$, $y \to z \to x$ and $z \to x \to y$). This is not acceptable because the averaged medium should not depend on the order of averaging.

We have developed a new orthorhombic representation of material heterogeneity. Heterogeneity of the medium in a finite-difference (FD) cell is represented by an averaged medium with an orthorhombic anisotropy with three axes of symmetry that are identical with the coordinate axes. An effective grid modulus is evaluated numerically as a volume orthorhombic average in a grid cell centred at the grid position of the corresponding stress-tensor component.

We numerically tested the orthorhombic representation for a complex 3D model of the Mygdonian sedimentary basin. We compared the FD seismograms with seismograms calculated using the spectral element method (SEM). For achieving sufficient accuracy of the reference SEM solution, we modified geometry of material interfaces so that the element faces exactly follow interfaces. For quantitative comparison of the FD and SEM seismograms we evaluated goodness-of-fit in envelope and phase.

The performed numerical tests show that the orthorhombic representation is more accurate than that developed by Moczo et al. (2002). As demonstrated by tests for 1D and 2D models, the orthorhombic representation is more accurate mainly for strong surface waves propagating along horizontal material interfaces.

The orthorhombic representation is applicable to modelling seismic wave propagation and earthquake motion in isotropic models with material interfaces and smooth heterogeneities using velocity-stress, displacement-stress and displacement FD schemes on staggered, partly-staggered, Lebedev and collocated grids.

ACKNOWLEDGMENTS

This work was supported in part by the Slovak Research and Development Agency under the contract number APVV-0271-11 (project MYGDONEMOTION), project Cashima and SIGMA (EDF, AREVA, CEA and ENEL). Part of the calculations were performed in the Computing Centre of the Slovak Academy of Sciences using the supercomputing infrastructure acquired in project ITMS 26230120002 and 26210120002 (Slovak infrastructure for high-performance computing) supported by the Research & Development Operational Programme funded by the ERDF. The SEM calculations were performed using HPC resources from GENCI-TGCC under grants (2013-046060, 2014-046060) and using the Froggy platform from the CIMENT HPC center of Grenoble Alpes University (https://ciment.ujf-grenoble.fr, last accessed March 2016) which is supported by the Rhône-Alpes region (GRANT CPER07_13 CIRA), the OSUG@2020 labex (reference ANR10 LABX56) and the Equip@Meso project (reference ANR-10-EQPX-29-01) of the Programme Investissements d'Avenir supervised by the Agence Nationale pour la Recherche. We appreciate critical and constructive comments by Wei Zhang and an anonymous reviewer.

REFERENCES

Backus, G. E. 1962. Long-wave elastic anisotropy produced by horizontal layering, *J. Geophys. Res.*, **67**, 4427–4440.

Bielak, J., Graves, R. W., Olsen, K. B., Taborda, R., Ramírez-Guzmán, L., Day, S. M., Ely, G. P., Roten, D., Jordan, T. H., Maechling, P. J., Urbanic, J., Cui, Y. & Juve, G., 2010. The

ShakeOut earthquake scenario: Verification of three simulation sets, *Geophys. J. Int.*, **180**, 375–404.

Bouchon, M., 1981. A simple method to calculate Green's functions for elastic layered media, *Bull. Seism. Soc. Am.*, **71**, 959-971.

Capdeville,Y. & Marigo, J.-J., 2007. Second order homogenization of the elastic wave equation for non-periodic layered media, *Geophys. J. Int.*, **170**, 823–838.

Capdeville, Y., Stutzmann, E., Wang, N. & Montagner, J. P., 2013. Residual homogenization for seismic forward and inverse problems in layered media, *Geophys. J. Int.*, **194**, 470–487.

Chaljub E., Cornou, C. & Bard, P.-Y., 2006. Numerical benchmark of 3D ground motion simulation in the valley of Grenoble, French Alps, Third International Symposium on the Effects of Surface Geology on Seismic Motion, Grenoble, France, 2006, August 30th – September 1st, paper number SB1, vol. 2.

Chaljub, E., Maufroy, E., Moczo, P., Kristek, J., Hollender, F., Bard, P.-Y., Priolo, E., Klin, P., de Martin, F., Zhang, Z., Zhang, W. & Chen, X., 2015. 3D numerical simulations of earthquake ground motion in sedimentary basins: testing accuracy through stringent models, *Geophys. J. Int.*, **201**, 90–111.

Chaljub, E., Moczo, P., Tsuno, S., Bard, P.-Y., Kristek, J., Käser, M., Stupazzini, M. & Kristekova, M., 2010. Quantitative comparison of four numerical predictions of 3D ground motion in the Grenoble Valley, France, *Bull. Seism. Soc. Am.*, **100**, 1427-1455.

Coutant, O., 1989. Program of numerical simulation Axitra. Res. Rep. LGIT (in French), Université Joseph Fourier, Grenoble.

Day, S. M., Bielak, J., Dreger, D. S., Graves, R. W., Larsen, S., Olsen, K. B. & Pitarka, A., 2003. Tests of 3D elastodynamic codes: Final report for Lifelines Project 1A02. Pacific Earthquake Engineering Research Center.

De Martin, F., 2011. Verification of a spectral-element method code for the Southern California Earthquake Center LOH.3 viscoelastic case, *Bull. Seism. Soc. Am.*, **101**, 2855–2865.

Hisada, Y., 1994. An efficient method for computing Green's functions for a layered half-space with sources and receivers at close depths, *Bull. Seism. Soc. Am.*, **84**, 1456–1472.

Hisada, Y., 1995. An efficient method for computing Green's functions for a layered half-space with sources and receivers at close depths (Part 2), *Bull. Seism. Soc. Am.*, **85**, 1080–1093.

Kristek, J. & Moczo, P., 2014. FDSim3D – The Fortran95 Code for Numerical Simulation of Seismic Wave Propagation in 3D Heterogeneous Viscoelastic Media. www.cambridge.org/moczo

Kristekova, M., Kristek, J. & Moczo, P., 2009. Time-frequency misfit and goodness-of-fit criteria for quantitative comparison of time signals, *Geophys. J. Int.*, **178**, 813-825.

Maufroy, E., Chaljub, E., Hollender, F., Kristek, J., Moczo, P., Klin, P., Priolo, E., Iwaki, A., Iwata, T., Etienne, V., De Martin, F., Theodoulidis N.P., Manakou, M., Guyonnet-Benaize, C., Pitilakis, K. & Bard, P.-Y., V. 2015. Earthquake ground motion in the Mygdonian basin, Greece: the E2VP verification and validation of 3D numerical simulation up to 4 Hz, *Bull. Seism. Soc. Am.*, **105**, 1398-1418.

Moczo, P., Kristek, J. & Galis, M., 2014. The finite-difference modelling of earthquake motions: Waves and ruptures, *Cambridge University Press*.

Moczo, P., Kristek, J., Vavryčuk, V., Archuleta, R.J. & Halada, L., 2002. 3D heterogeneous staggered-grid finite-difference modeling of seismic motion with volume harmonic and arithmetic averaging of elastic moduli and densities, *Bull. Seism. Soc. Am.*, **92**, 3042-3066.

Muir, F., Dellinger, J., Etgen, J. T., & Nichols, D., 1992. Modeling elastic fields across irregular boundaries, *Geophysics*, **57**, 1189–1193.

Schoenberg, M., & Muir, F., 1989. A calculus for finely layered anisotropic media, *Geophysics*, **54**, 581–589.